IEEE Access
Multidisciplinary | Rapid Review | Open Access Journal

Received 26 August 2023, accepted 28 September 2023, date of publication 16 October 2023, date of current version 2 November 2023.

Digital Object Identifier 10.1109/ACCESS.2023.3324965

RESEARCH ARTICLE

Virtual Lidar Sensor Intensity Data Modeling for Autonomous Driving Simulators

DONG-JU LEE, JIUNG IM, (Graduate Student Member, IEEE), AND JONG-HOON WON, (Member, IEEE)

Department of Electrical and Computer Engineering, Inha University, Incheon 22212, South Korea

Corresponding author: Jong-Hoon Won (jh.won@inha.ac.kr)

This work was supported by the Institute of Information & Communications Technology Planning & Evaluation (IITP) funded by the Ministry of Science and ICT (MSIT) of the Korean Government through the Development of Reality-Virtual Information Convergence and Edge-Based Autonomous Driving Simulation Software Technology under Grant No. 2021-0-01414.

ABSTRACT Autonomous driving simulators are an effective tool for developing autonomous driving algorithms so that they are widely used in research and development. However, the similarity of the virtual model to reality is closely related to the validity of the simulation results. Therefore, analyzing the characteristics of real sensors is necessary for mathematical modeling of virtual sensors in autonomous driving simulators. This paper presents a virtual lidar that has a high fidelity operating similarly to reality in the sensor modeling. The intensity variable factors which represents the strength of the received signal relative to the transmitted signal are effectively used for improving the fidelity of virtual lidar with a low computing power. The proposed virtual lidar is implemented in an autonomous driving simulator to show its feasibility by comparing with the existing virtual lidar. Specifically, the paper focuses on modeling intensity data with an aim to exhibit trends similar to the intensity measurement results of real lidar, compared to conventional modeling methods. The proposed virtual lidar is implemented in an autonomous driving simulator to demonstrate its feasibility by comparison with existing virtual lidar. As a result, there was an 89.21 percent improvement in the average intensity within the region of interest compared to the conventional modeling method.

INDEX TERMS Driving simulator, fidelity, lidar sensor model, intensity, sim2real.

I. INTRODUCTION

In the development of autonomous driving technology, accurately perceiving the positions of pedestrians and other vehicles in the vicinity is directly related to the safety of passengers and nearby people. In this context, sensors such as cameras, radars, and lidars are widely used for a driving environment perception capability of autonomous driving vehicles. Among them, lidars measure using the transmission and reception of laser signals, and acquire point cloud data (PCD) with excellent spatial resolution in centimeters, providing 3D spatial information. Due to the structural and functional characteristics of the sensors mentioned above, there is a trend toward developing autonomous driving perception capabilities through sensor configurations that combine the strengths and weaknesses of each sensor [1].

Meanwhile, evaluating and verifying the driving safety of autonomous driving functions is a task as important developing the autonomous functions themselves. Furthermore, evaluating and verifying high level autonomous driving functions in all test cases of real world environments incurs high costs and time consumption. Therefore, driving simulators have been considered as a tool for evaluating and verifying autonomous driving systems, as they can be used safely, inexpensively, and with reproducible results [2]. However, since there are differences between driving simulators and real-world environments, many researches are being conducted to reduce the discrepancy between virtual models and reality. This is commonly referred to as the Simulation-to-Real (Sim2Real) problem, aiming to transfer knowledge from simulation to real-world situations in areas such as driving scenarios [3], vehicle dynamics [4], and sensor modeling [5], [6]. In this context, co-simulation software, notably AVL Model.CONNECT, has been recognized for its role in

The associate editor coordinating the review of this manuscript and approving it for publication was Wei Wei.

addressing this challenge. It facilitates the integration of various simulation methodologies, helping to streamline the transition from virtual models to real-world scenarios. Building on this foundation, our research narrows its focus specifically to the development and optimization of virtual lidar sensor modeling. A precise and detailed representation of virtual lidar systems is crucial for enhancing the authenticity of simulations, bridging the gap between simulated and real-world environments. Analyzing the characteristics of real sensors is necessary for developing virtual sensors. A lidar measures the position of a specific point based on the Time of Flight (ToF) principle, which calculates the distance by transmitting a signal at a certain angle, reflecting off a specific point, and receiving the signal based on the elapsed time. Lidars can be differentiated based on their signal form and emission method. In this study, we focus on the narrow-pulsed signal lidar. This type is prevalent in the market and functions by rotating either its body or its internal mirrors using a rotor [7].

Rosenberger et al. [8] studied the mechanical operation characteristics of the Ibeo LUX 2010, which operates using a narrow-pulsed signal through a rotor. They confirmed that the LUX 2010 has a zipper shaped measurement range due to different measurement directions depending on the vertical scan layer and horizontal resolution. They also emphasized the need to analyze and reflect the real sensor's operational characteristics in the development of virtual lidar. Furthermore, Schaermann et al. [9] proposed a method for evaluating virtual lidar that is implemented in Vires' driving simulator, Virtual Test Drive (VTD). They suggested comparing the point position measurement results of the sensor by reproducing the same driving scenario in both real and virtual environments.

In virtual lidar development research, Rosenberger et al. [10] proposed a ray-casting based virtual lidar, considering signal divergence, signal-to-noise ratio (SNR), and measurement range due to sensor structure. To evaluate the proposed virtual lidar, they defined a lidar system flowchart based on object detection function for the classification of interfaces. They also presented a method to assess the fidelity of virtual lidar implementation, not only by comparing point positions but also by correlating with surrounding object list information in the scenario. Linnhoff et al. [11] emphasized the importance of not only high fidelity but also the computational speed for driving simulators. In their study, they demonstrated that phenomenological based virtual lidar data, modeled using ray-tracing techniques for high fidelity virtual lidar and surrounding object list information in the scenario, could be generated 200 times faster. In this case, the phenomenological based virtual lidar took into account field-of-view limitations and atmospheric attenuation. However, existing virtual lidar research has primarily focused on the position measurement function, with relatively little attention given to modeling the intensity, which represents the reflectivity of the measured points.

Since intensity can reflect the reflective properties of objects, unlike position measurement results, Hata & Wolf [12] explained that it can be used to detect road markings such as solid lines, dashed lines, and crosswalks while driving. In addition, a method for estimating the current position while driving using intensity has been proposed. Wang et al. [13] described a method for detecting the types of surrounding objects in a driving environment using both intensity and position information from the PCD. Through these two studies, it can be seen that intensity measurement is useful for developing lidar based autonomous driving functions, and there is a need for intensity information in driving simulator virtual lidar.

In this study, we focus on developing a high-fidelity virtual lidar that operates similarly to its real-world counterpart, particularly in the sensor modeling aspect of the Sim2Real problem. For this endeavor, our investigative process utilizes the open-source driving simulator CARLA [14], renowned for its modular architecture. This architecture supports the implementation of various models, including traffic, scenario, road, and sensor modules, each customizable to meet the demands of a myriad of tasks associated with autonomous driving development and verification. Furthermore, CARLA allows for meticulous adjustments to experimental scenarios by enabling modifications to factors such as weather conditions, object positioning, surface color, and surface materials. Importantly, CARLA comes equipped with a pre-implemented lidar model within its simulation environment, providing a convenient baseline for the comparison and validation of our proposed virtual lidar system. Utilizing internal scenario parameters of CARLA, we analyze the intensity variable factors vital for improving the fidelity of the virtual lidar.

Unlike previous studies, our proposed virtual lidar is keenly focused on the intensity parameter, which is crucial as it represents the strength of the received signal relative to the transmitted signal. The objective is to achieve a high-fidelity virtual lidar that requires low computing power, accomplished by effectively utilizing weather parameters and object databases configurable in the driving simulator. The paper is organized as follows: First, an introduction to the analysis of real lidar and previous research on virtual lidar is provided. Next, we define the lidar functional flow and divide the interfaces to elucidate the intensity modeling, which is the focal point of our research, describing the causes of measurement errors and the intensity variable factors in the process. Subsequently, we delve into the explanation of the virtual lidar implemented in CARLA, presenting comparison experiments and results between the existing virtual lidar and our proposed system. The paper concludes with final remarks and conclusions.

II. LIDAR ANALYSIS

A. SYSTEM

For autonomous driving functions, a lidar measures the surroundings using infrared signals with a wavelength of 850∼1550nm, which is non visible light, while considering

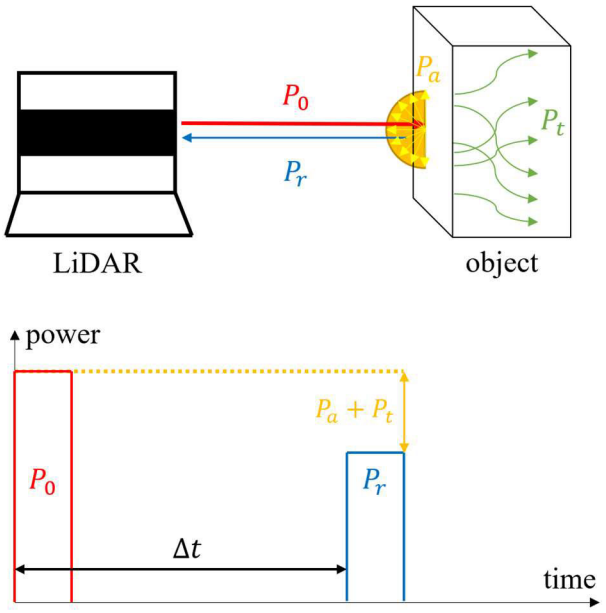

FIGURE 1. Lidar signal acquisition principle.

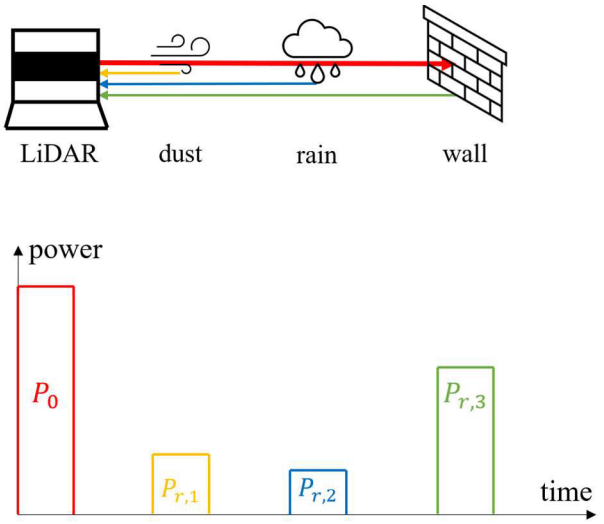

FIGURE 2. Example of lidar multi echo signal measurement.

the safety of people's eyes around it, and operating at a limited peak power. In this case, the arbitrarily transmitted narrow pulsed signal P_0 to measure surrounding objects is shown in Fig. 1, where P_r is the signal reflected by surrounding objects and received, P_a is the signal that has disappeared due to diffuse reflection, and P_t is the signal absorbed and converted into heat. The distance measurement is calculated by the difference between the transmission time and reception time, Δt, and the speed of light, c, where the distance d is $c\Delta t/2$. There are several methods used for measuring the reflectivity characteristics of objects. For an example, Ibeo's pulse width method outputs the pulse width length of the received P_r signal from the object [15]. For another example, Velodyne's intensity method outputs the intensity value by applying the reflectance correction factor provided by the National Institute of Standards and Technology to the ratio of the transmitted signal's strength to the received signal's strength [16].

In a lidar, the transmitted signal can diverge as the flight distance increases, allowing multiple objects to be measured simultaneously. Glass, rain, fog, and dust may also cause multiple received signals. LUX 2010 names each of these signals as an 'Echo'. An example of multiple Echo occurrences is shown in Fig. 2, and each has a unique position value and reflectivity value [15]. In the case of VLP-16, specific signals among multiple Echo signals can be received through sensor settings [16]. There are three representative specific reception modes: the first signal reception, the last signal reception, and the strongest signal reception. The first signal reception is a mode that receives the signal measured first, such as receiving the signal $P_{r,1}$ due to dust in Fig. 2. The last signal reception is a mode that receives the signal measured last, such as receiving the signal $P_{r,3}$ due to the wall in Fig. 2. The strongest reception is a mode that receives the signal with the highest intensity, like the last signal reception, receiving the signal $P_{r,3}$ due to the wall in Fig. 2. Additionally, there is a Dual reception mode that combines the above modes.

Based on the above analysis and the research of Rosenberger et al. [10], focusing on object detection functionality, the lidar system interface in this paper is as shown in Fig. 3. Interface (IF)1 has the same message structure as the LUX 2010's sensor output interface, including multiple Echo data and returning object reflectivity in a Pulse width form. IF2 is identical to the VLP-16's sensor output interface and returns one signal among multiple Echo signals through reception mode settings and internal sensor processing. In this paper, we handle the strongest signal reception mode. The arbitrary point position values measured by a lidar are output in a spherical coordinate system with vertical channel ω, horizontal angle α, and measured distance d. IF3 converts the spherical coordinate system to a Cartesian coordinate system in the form of $[x, y, z]$ centered on the lidar, excluding intensity and converting location information only into a 3D array PCD. IF3 represents the lidar 3D spatial measurement functionality focused on in the previous research, and when using multiple lidars, it is aligned based on the vehicle coordinate system. Finally, IF4 is an object list information with a completed PCD signal processing such as point clustering, object classification, object detection, and tracking. It includes information such as the type of object, the central coordinates of the object, and the size of the object bounding box. It can be extended to include messages for arbitrary objects identifier for tracking, tracking progress, and object heading direction.

B. MEASUREMENT ERROR

High fidelity virtual lidar should apply measurement errors that occur in reality. Measurement errors refer to cases where

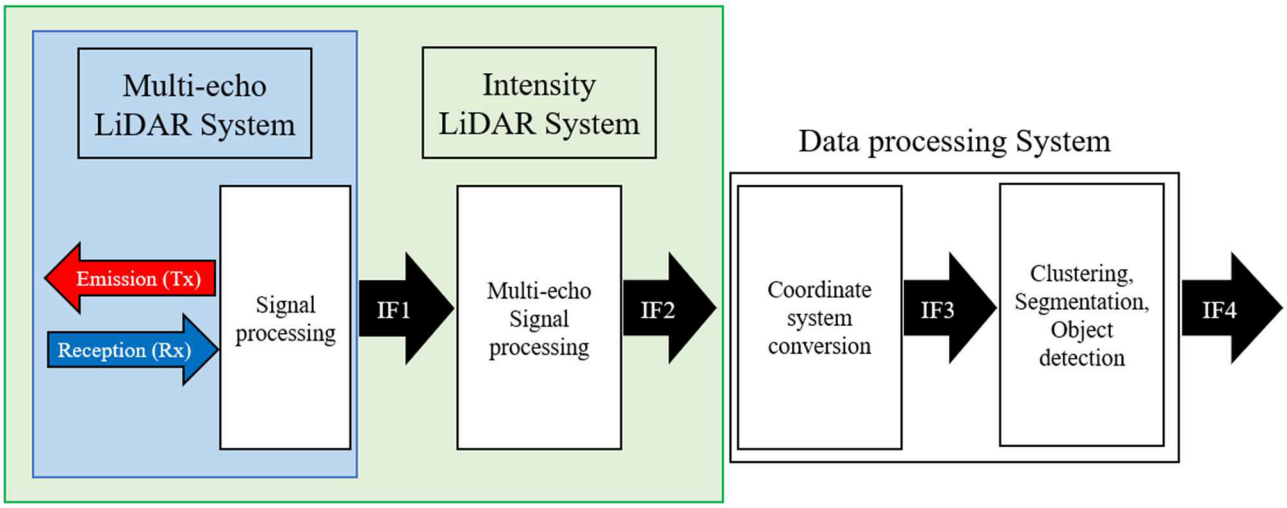

FIGURE 3. Lidar system interface definition.

points in the PCD are not measured or the position of points is measured differently from the actual location. In this study, we deal with the effects of weather and rotor rotation. First, Vargas Rivero et al. [17] classified weather effects as dirt or insect cover on the lidar cover, water (or snow) cover, signal scattering, and absorption during raindrops (and/or fog, dust), wet state of the measured target object (i.e., snow covered state, dust covered state), and changes in measurement environment lighting.

Filgueira et al. [18] conducted experiments on the impact of rainfall on lidar measurement results. Rainfall was measured in liters per square meter per hour, using the unit $l/\left(m^2h\right)$. They placed the VLP-16 on the sidewalk next to the road for 60 days and measured common elements in driving environments such as concrete walls, road surfaces, lane control poles, traffic signs, and building information signs. The impact on the measurement results was compared using the number of point per rainfall, the distance to the points (location information) per rainfall, and the average intensity of the Region of Interest (ROI) per rainfall for each object by setting the ROI. The experiment showed that as the intensity of the rain increased, lidar's PCD point loss and changes in average intensity were observed.

Kutila et al. [19] aimed to develop a lidar with low weather impact and experimented with the feasibility of measurement using high peak power in strong fog conditions. Since the peak power cannot be increased for the 905nm wavelength, which is close to visible light (400∼700nm), due to the eye safety issues for people around, they focused on the 1550nm wavelength, which allows for higher peak power. In this process, they measured the impact of weather related measurement results in VLP-16 and LUX2010, which will be used to evaluate the 1550nm wavelength lidar to be developed later. Here, the intensity of fog was measured using the road visibility meter unit, and the intensity of rain was measured using the vertical height of rain per hour [mm/h] unit. They measured ideal experimental control group situations without rain and fog, heavy rain situations with 33mm/h, mild fog situations with road visibility of 15m, and strong fog situations with road visibility of 40m. The experiment found that while rain also affects lidar measurements, the impact of fog is greater, and the loss of PCD points increases depending on road visibility in foggy conditions.

Rotor rotation effects occur when creating a single PCD, as the lidar body or the internal mirror used to change the direction of the signal transmitter and receiver rotates 360° to aggregate measurement results. This happens because the lidar or surrounding objects like vehicles move during the measurement. This creates PCDs similar to motion blur phenomena that occur in cameras. Research is being conducted to correct PCDs for distortions caused by such lidar movement by fusing sensor data from Global Positioning Systems and Inertial Measurement Units [20].

III. INTENSITY DATA VARIABLE

Building upon the work of Linnhoff et al. [11], which utilized object list data from a driving simulator for virtual lidar implementation, this study seeks to analyze the factors affecting the intensity of actual lidar measurements about target objects. Specifically, this research investigates the influence of reflection characteristics and color of the measured objects on their reflectivity. Surface reflection characteristics can be categorized into three types: specular reflection, diffuse reflection, and retroreflection. Considering a scenario in which a signal impinges upon the surface of an object at an angle θ, the following reflection phenomena can be observed: first, specular reflection occurs when the signal is reflected in the opposite direction $(180° - \theta)$ and is commonly observed on smooth surfaces, akin to a mirror; second, diffuse reflection scatters the incident signal in multiple directions

(a) (b)

FIGURE 4. Reflection characteristic experiment: (a) diffuse reflector, (b) retroreflector.

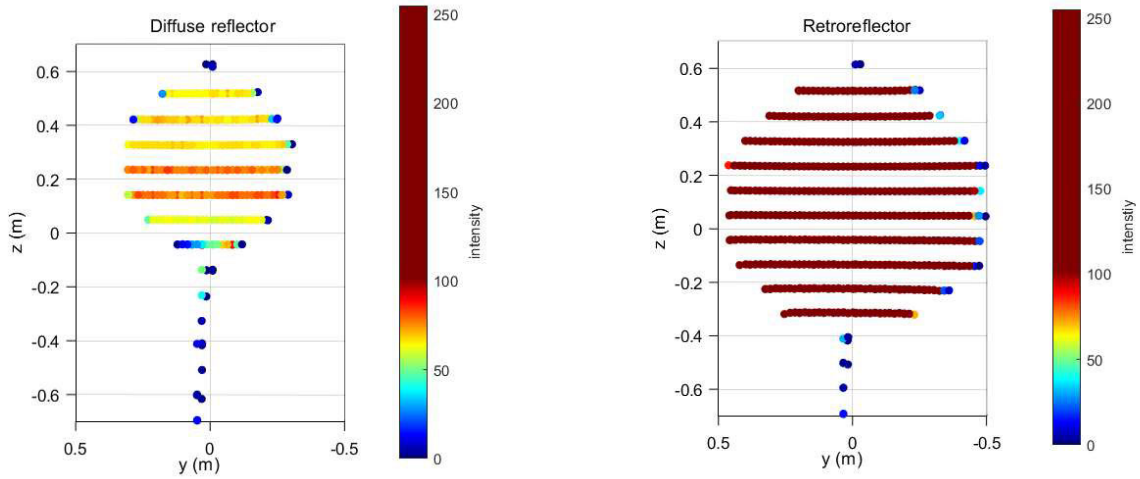

(a) (b)

FIGURE 5. Test results for reflection characteristics through VLP-16: (a) diffuse reflector, (b) retroreflector.

and typically manifests on rough surfaces as a prevalent reflection form; third, retroreflection reflects the signal at the same incident angle θ and transpires on surfaces composed of special retroreflective materials.

The intensity of the VLP-16 is an 8-bit unsigned integer with no specific SI unit, ranging from 0 to 255. This digital number represents the ratio of received signal strength to the emitted signal strength for a pulse sent to detect objects, serving as a post-processed result of the received pulse width. The intensity value reflects the object's characteristics: values from 0 to 100 correspond to 0 to 100% reflectance measurements on diffuse reflective surfaces, whereas values from 101 to 255 are indicative of retroreflective surfaces, with values approaching 255 denoting ideal reflectance forms. Utilizing this information, object level data can be employed for classification, necessitating the incorporation of this phenomenon in virtual lidar. Consequently, experiments are conducted to assess the performance of the actual sensor depending on the object's surface reflection characteristics.

The experimental sensor used in this paper is the VLP-16, and measurements were taken of traffic signs coated with diffuse reflective surfaces and traffic signs coated with retroreflective surfaces under identical weather conditions. Taking into account the horizontal measurement range of the VLP-16 and the distance to the measured objects, the reflection characteristic measurement environment was set up as shown in Fig. 4. The obtained PCD from the measurements was used to set the ROI around the traffic sign signals, and the intensity values were represented in a graph as shown in Fig. 5. The intensity values closer to 0 are represented in blue, while those closer to 255 are represented in red.

The experiment showed that there was a significant difference in intensity values between diffuse and retroreflective

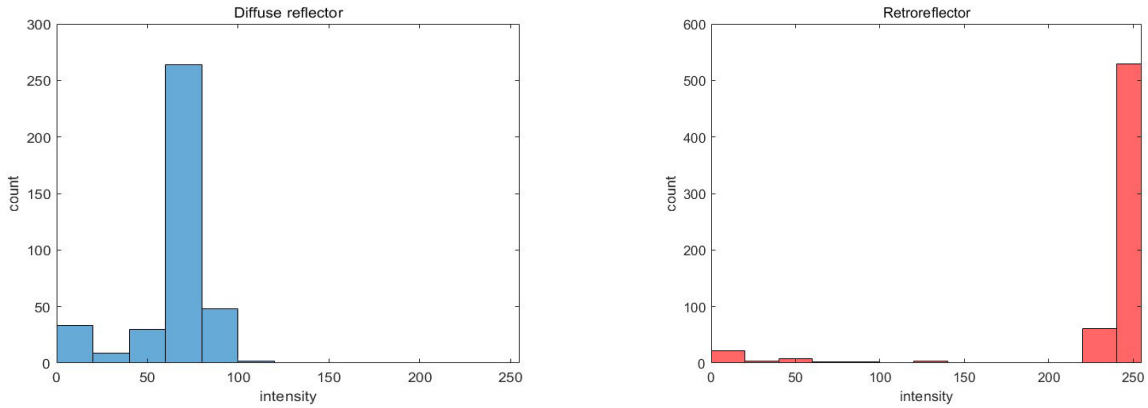

(a) (b)

FIGURE 6. Intensity cumulative distribution by reflection characteristics through VLP-16: (a) diffuse reflector, (b) retroreflector.

(a) (b) (c)

FIGURE 7. Color characteristic experiment: (a) red, (b) yellow, (c) blue.

TABLE 1. Intensity difference by reflection characteristics.

	Diffuse reflector	Retroreflector
Number of Point	386	842
Total intensity	24423	200766
Average intensity	63.27	238.73

measurements, and it was possible to distinguish between the traffic sign panel and the traffic signpost in the diffuse reflection measurement results. The cumulative distribution of intensity based on reflection characteristics is shown in Fig. 6. For diffuse reflection, the intensity of traffic signs was found to be between 60 and 80, while for retroreflection, the intensity was between 240 and 255. For quantitative verification, Table 1 is composed of ''Number of point'', ''Total intensity'', and ''Average intensity''. Specifically, ''Number of point'' represents the total count of all measured points within the ROI. ''Total intensity'' refers to the cumulative sum of intensity values of all these measured points. Finally, ''Average intensity'' is derived by taking the sum of intensity values of all points within the ROI and dividing it by the number of point.

Considering that color may influence reflectivity, it was hypothesized that changes in an object's surface color would affect intensity as well. This assumption was tested in a previous study [21] by examining the variations in intensity based on color. In this experiment, the VLP-16 sensor was employed to investigate the differences in intensity between panels of different colors, made of the same styrofoam material. The results from the yellow and black panels in the study revealed differences in intensity values, confirming that color does indeed impact intensity.

To incorporate the effect of surface color into virtual lidar, the measurement environment was configured as shown in Fig. 7. Red, yellow, and blue traffic control bollards, which are commonly seen in driving environments, were measured using the VLP-16 sensor. The ROI was set around the bollards, and the PCD results based on intensity measurements are presented in Fig. 8. Although the differences were less pronounced compared to those observed for reflection characteristics, it was evident that intensity varied depending on the color. The cumulative intensity distribution by color, as shown in Fig. 9, indicated that the strongest intensity values were measured for the blue bollards. For quantitative verification, the total number of point measured based on the ROI, the sum of intensities, and the average intensity results are presented in Table 2.

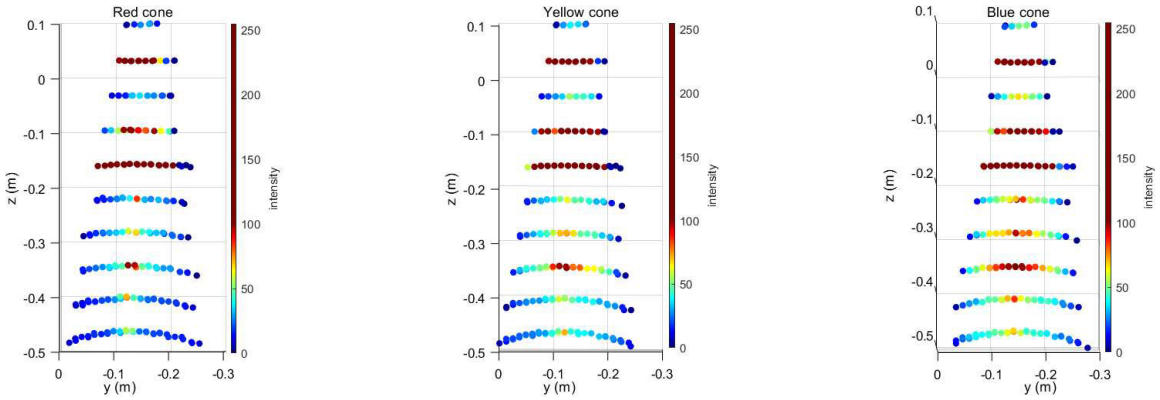

FIGURE 8. Test results for measuring color characteristic through VLP-16: (a) red, (b) yellow, (c) blue.

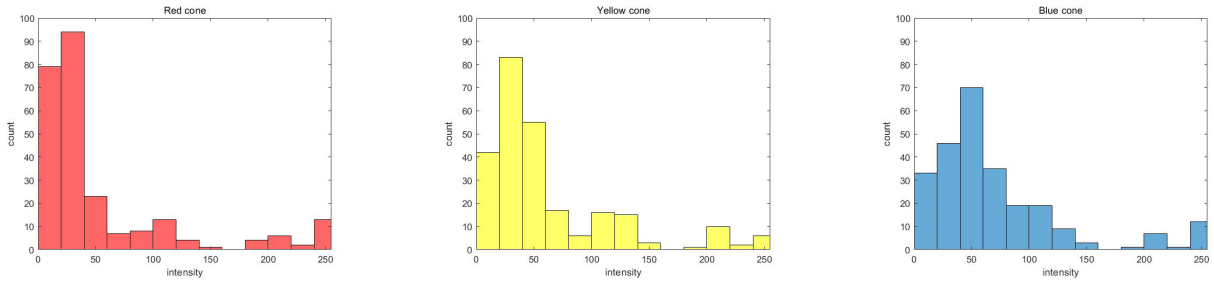

FIGURE 9. Intensity cumulative distribution by reflection characteristics through VLP-16: (a) red, (b) yellow, (c) blue.

TABLE 2. Intensity difference by color characteristics.

	Red cone	Yellow cone	Blue cone
Number of Point	16800	19904	22016
Total intensity	13568	15518	17673
Average intensity	53.417	60.617	69.306

IV. VIRTUAL LIDAR SIMULATION

For the validation of the proposed virtual lidar, a driving simulator, CARLA, is used as a simulation platform. CARLA provides assets such as road segments, vehicles, pedestrians, buildings, trees, and various traffic signals and signs for configuring driving scenarios. Additionally, it offers virtual sensor models simulating real autonomous driving sensors, including cameras, lidar, radar, GPS, and IMU. Semantic sensors for feature development, such as collision detection sensors, lane detection sensors, driving stability sensors, object type segmentation image sensors, and object type segmentation lidar, are also available. The CARLA lidar is implemented using the ray-casting technique, and its input and output parameters are in accordance with CARLA [14]. As evident from the CARLA lidar input parameters, the default settings for a realistic sensor include a 45% random point deletion probability and a 40% probability of deleting points with an intensity of 0. However, in this study, these error models are set to 0%. The raw data output from CARLA lidar is a four dimensional array representing the position of the measured point and reflectivity, composed of $[x, y, z, intensity]$. The intensity generation model of CARLA lidar is given by Equation (1).

$$I = e^{-a \cdot d} \cdot I_0 \tag{1}$$

where I represent the intensity measured by CARLA lidar, a is the atmospheric attenuation coefficient, d is the distance between the measured object and the lidar signal receiver, and I_0 is the original intensity generated by the measured object. From this Equation (1), it can be observed that the CARLA lidar only considers the 'loss during the signal's travel from the object to the lidar signal receiver' in intensity generation. However, the actual lidar intensity measurement is influenced by 'loss during the signal's travel from the lidar transmitter to the object', 'loss during the signal's travel from the object to the lidar signal receiver', 'measured object surface reflection angle', 'measured object surface

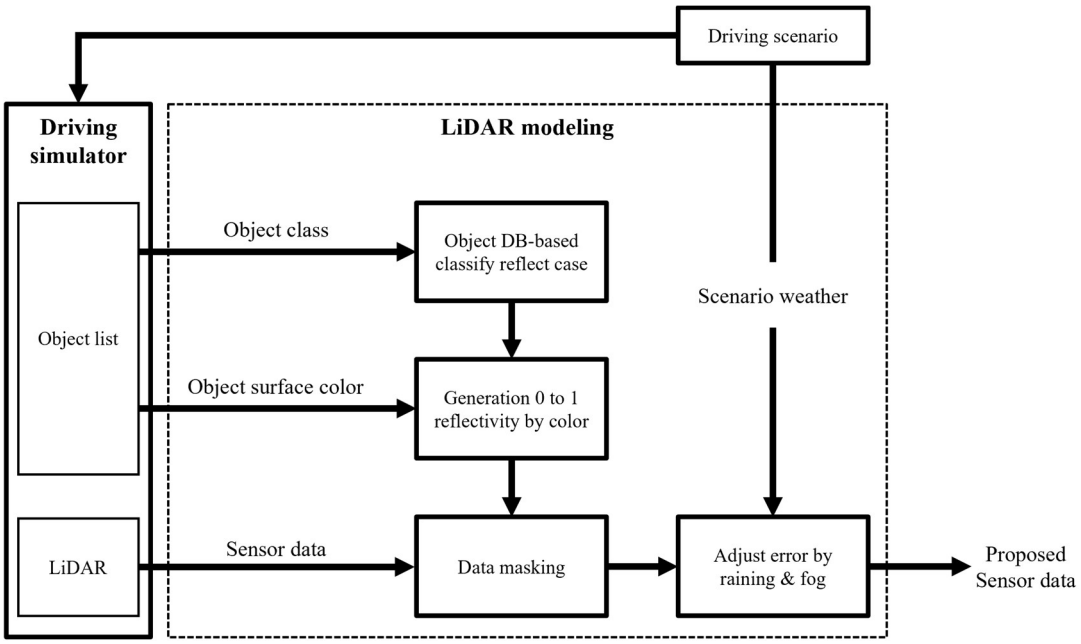

FIGURE 10. Proposed LiDAR modeling method.

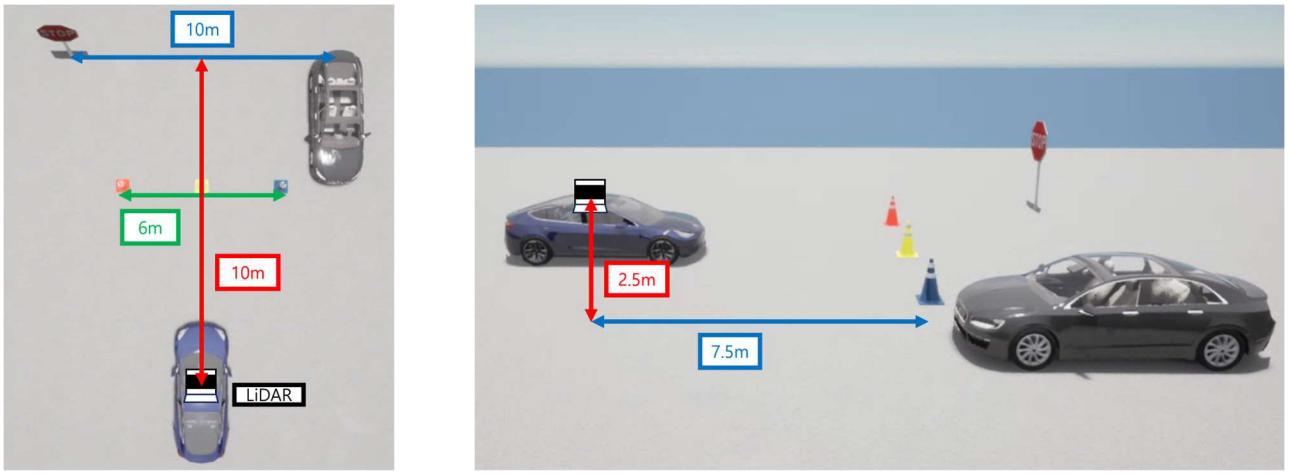

(a) (b)

FIGURE 11. Virtual Lidar weather impact comparison experimental environment: (a) top view, (b) side view.

TABLE 3. Intensity difference by weather impact comparison experiment.

	CARLA Lidar	reference weather	heavy rain	dense fog	heavy rain & fog
Number of Point	1735	1735	1745	352	1006
Total intensity	435760	23705	60242	11425	32488
Average intensity	251.303	13.671	34.542	32.55	32.326

characteristics', 'measured object surface color', and 'measurement environment weather'. Therefore, we propose a virtual lidar with increased fidelity that reflects the effects of 'measured object surface characteristics', 'measured object surface color', and 'measurement environment weather' without increasing computational complexity, by utilizing the object information and driving scenario weather data provided by CARLA in real time.

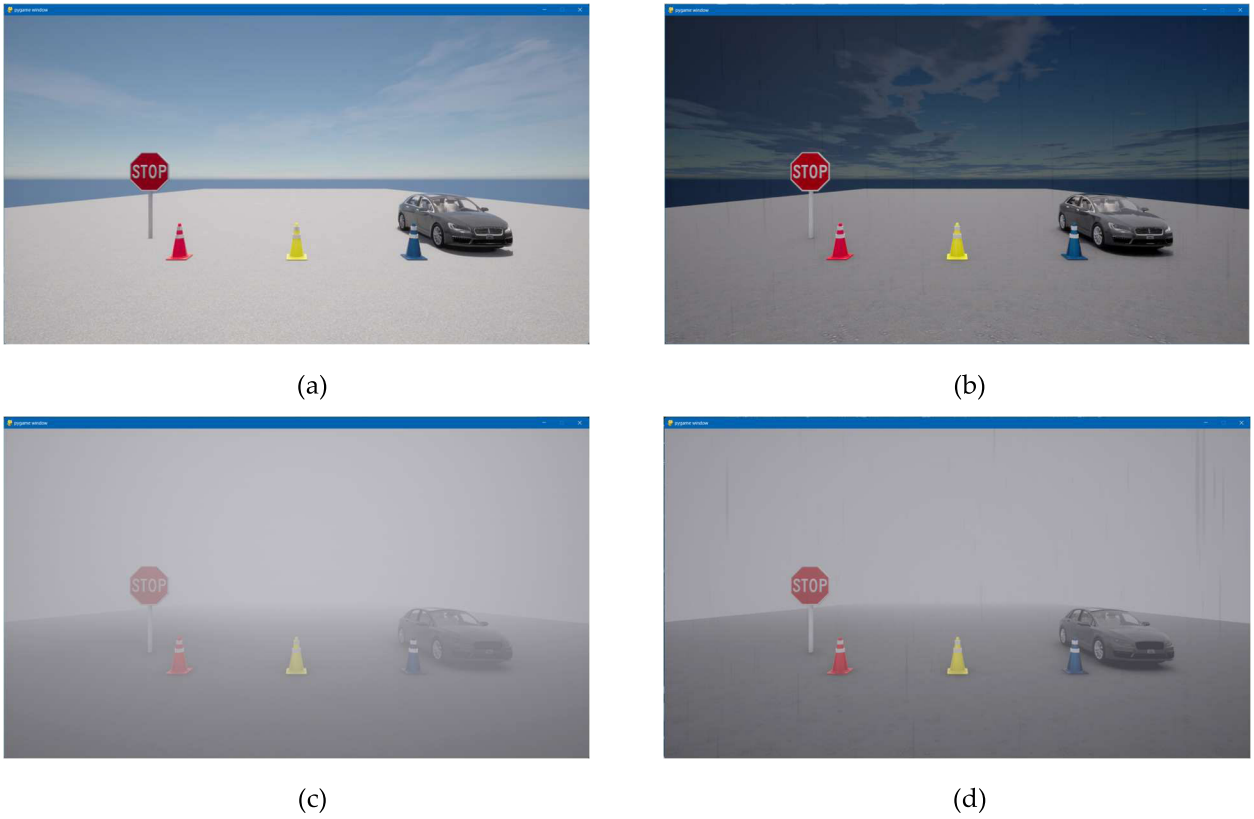

FIGURE 12. Virtual Lidar's weather impact comparison experiment image: (a) reference weather (rain intensity $R = 0$, fog intensity $F = 0$), (b) heavy rain ($R = 1$, $F = 0$), (c) dense fog ($R = 0$, $F = 1$), (d) heavy rain & fog ($R = 0.75$, $F = 0.5$).

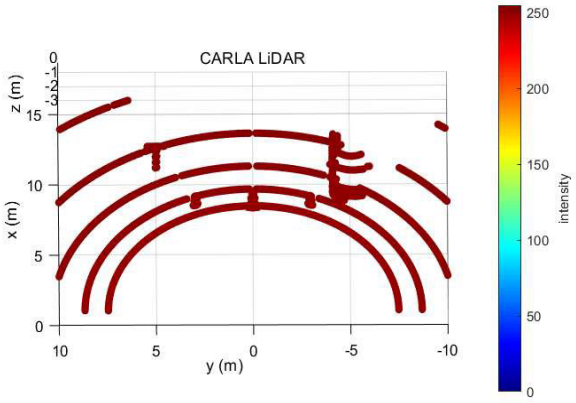

FIGURE 13. PCD acquisition results of weather impact comparison experiment of CARLA Lidar.

Fig. 10 presents the block diagram of the proposed virtual lidar system, operating as follows: The system employs CARLA's semantic lidar for object segmentation, recognizing surfaces such as metal, wood, and retroreflective materials. Once surfaces are identified, they are compared with a database generated from actual lidar measurements, yielding intensity values ranging from 0 to 255. Surface color information is extracted from the object model, and a color reflectance correction coefficient, based on empirical measurements, is applied to the intensity value. To simulate lidar measurement errors, the system utilizes the simulator's weather parameters, including rain intensity (R, varying from 0 to 100%) and fog intensity (F). For rain, White Gaussian (WG) noise with a mean of 0 and a standard deviation between 0 and 0.2 is applied to the PCD, with the standard deviation increasing linearly with R. For fog, a random point deletion probability between 0 and 0.8 is applied to the PCD based on the value of F, following the experiment by Kutila et al. [19], which demonstrates that more points are randomly removed from the PCD under heavier fog conditions. Similarly, the system applies WG noise with a mean of 0 and a standard deviation between 0 and 0.2 to the PCD by the value of F. If both rain and fog are present, the standard deviation of WG is applied based on the higher value between R and F.

In summary, the proposed virtual lidar system adjusts the intensity value of the existing PCD based on empirical measurement results when surface characteristics and color change. Subsequently, errors induced by rain and fog are incorporated into the generated PCD. This approach leverages the simulator's information without adding computational complexity, thus creating more realistic PCDs.

The experimental environment includes recursive reflective surfaces of traffic signs, road regulation bollards, and

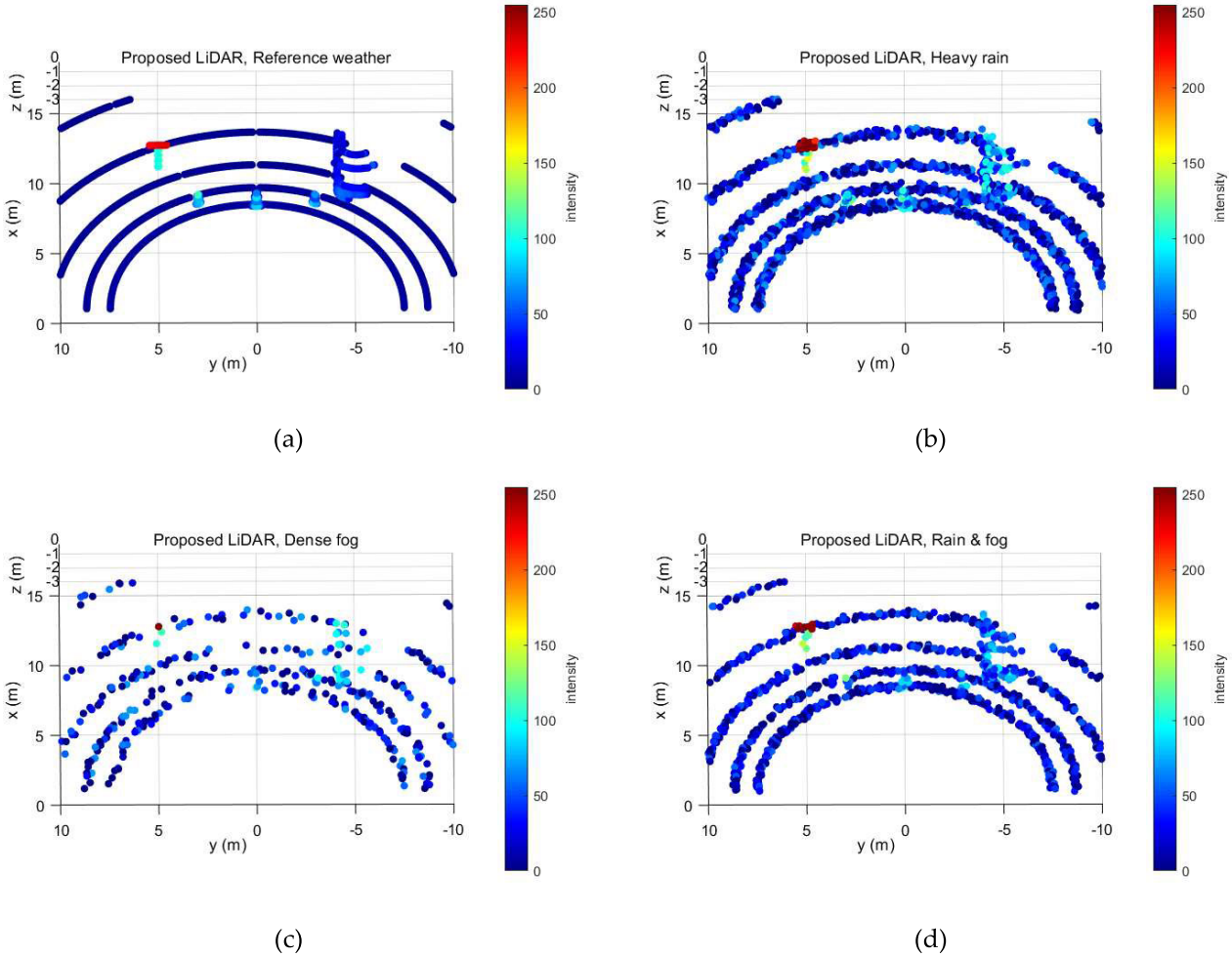

FIGURE 14. PCD acquisition result of weather impact comparison experiment of proposed Lidar: (a) reference weather (rain intensity $R = 0$, fog intensity $F = 0$), (b) heavy rain ($R = 1$, $F = 0$), (c) dense fog ($R = 0$, $F = 1$), (d) heavy rain & fog ($R = 0.75$, $F = 0.5$).

vehicles typically encountered in driving scenarios. The experimental environment in Fig. 11 measures four conditions by altering the weather parameters R and F, as illustrated in Fig. 12. The first condition represents a clear day, the second condition simulates heavy rain, the third represents heavy fog, and the fourth condition encompasses a combination of rain and fog.

Since the conventional CARLA lidar is not affected by weather conditions, its measurement results are shown in Fig. 13. The first condition represents a clear day, the second condition simulates heavy rain, the third represents heavy fog, and the fourth condition encompasses a combination of rain and fog. However, the proposed lidar, as in previous studies, experiences measurement errors due to rain and fog, with results displayed in Fig. 14. The comparison experiment environment shows the number of point, total intensity, and average intensity in Table 3. This demonstrates that the proposed method successfully simulates measurement errors caused by weather conditions compared to CARLA lidar.

Especially in the comparative experiment on measurement results according to weather changes such as rain and fog, using the real lidar from [19], it was found that there was no significant change in the total number of points during heavy rain. However, there were substantial changes in the total number of points in foggy conditions. By comparing the number of points in 'reference weather' and in adverse weather conditions as shown in Table 3, it is evident that the total number of points changes depending on the weather, with foggy conditions having a particularly significant impact on the number of points. Furthermore, the results measured using the lidar modeling method proposed in the study show that while the average intensity is 13.671 in clear 'reference weather' conditions, it ranges between 30 to 35 in adverse weather conditions like heavy rain and dense fog, indicating that these conditions influence the intensity measurement results.

To validate the implementation fidelity of the proposed virtual lidar, identical real and virtual measurement experiment

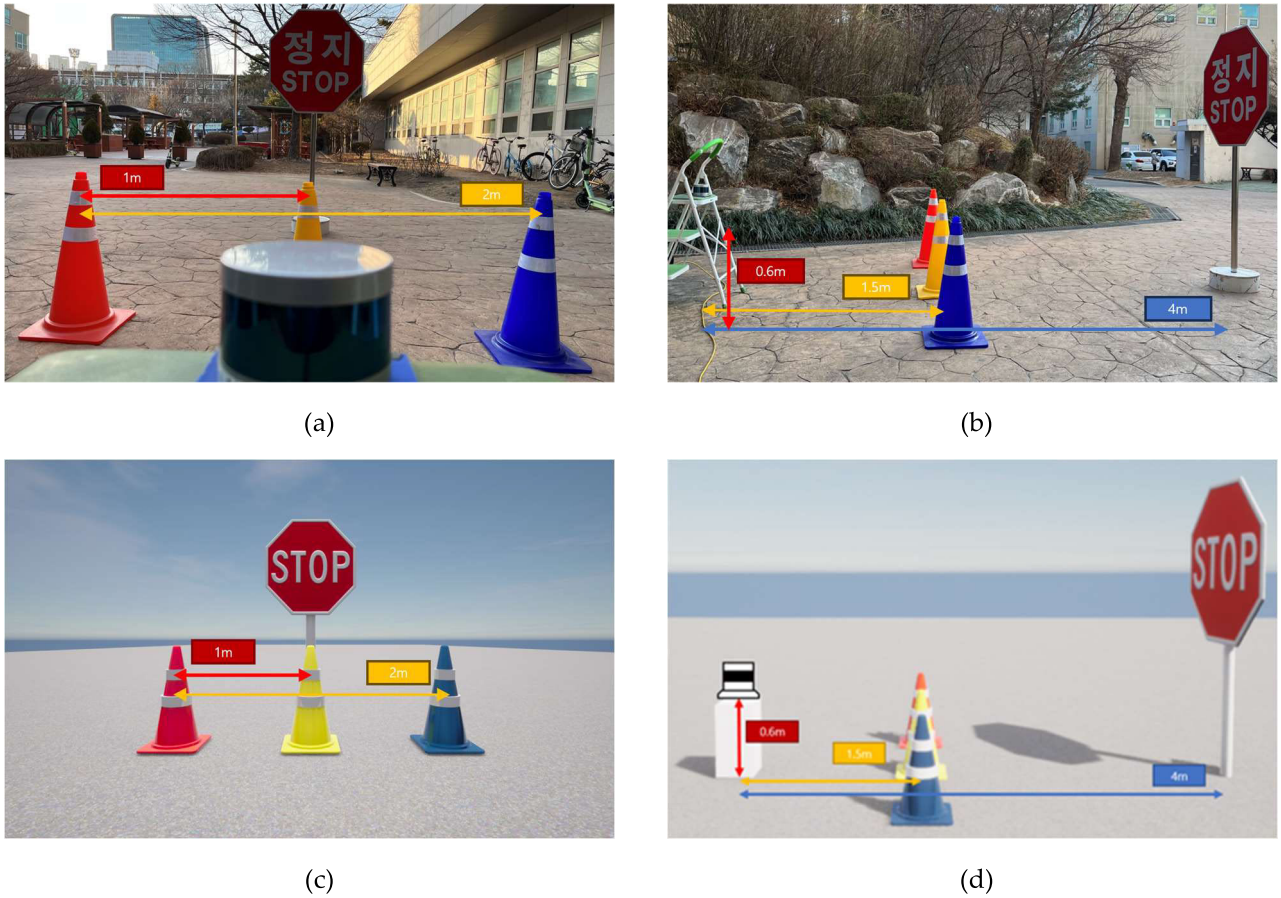

FIGURE 15. Virtual Lidar fidelity comparison experimental environment: (a) Real environment front view, (b) Real environment side view, (c) Virtual environement front view, (d) Virtual environment side view.

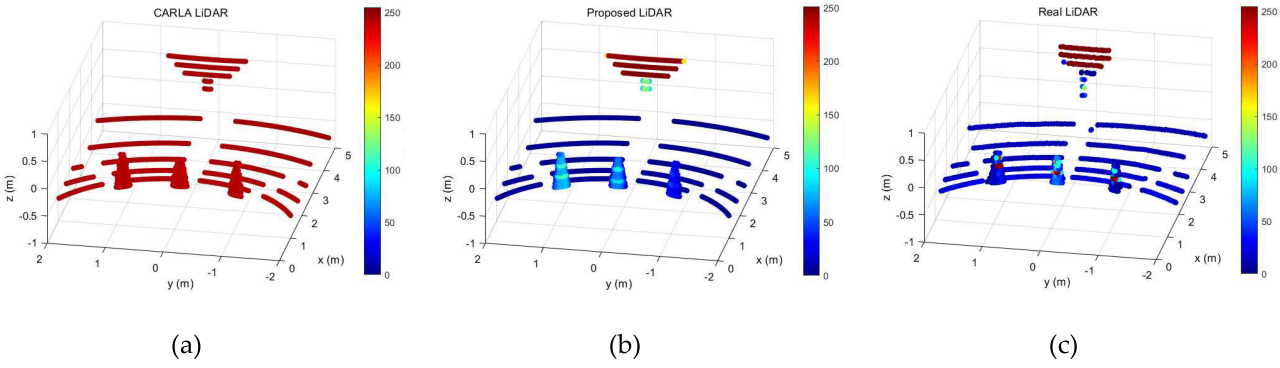

FIGURE 16. PCD acquisition results of fidelity comparison experiment: (a) CARLA Lidar, (b) Proposed Lidar, (c) Real Lidar.

environments were set up, as shown in Fig. 15. The implementation fidelity validation experiment measured data using the VLP-16, proposed virtual lidar, and CARLA lidar, with the resulting PCD shown in Fig. 16. Comparing the PCD maps, it appears that there is a minimal difference between the VLP-16 PCD and the proposed lidar PCD. To quantify these differences, the number of point, total intensity, and average intensity for each lidar PCD are displayed in Table 4. The results show that there is a nearly twofold difference in the number of point between the real and virtual lidars. Comparing the proposed method with the conventional CARLA lidar, it is evident that the intensity of the proposed method is more similar to reality.

To further investigate the differences in intensity, the cumulative intensity distribution for each lidar is shown in Fig. 17. The real lidar and the proposed method's cumulative intensity distributions are similar, confirming the effectiveness of the proposed method in enhancing implementation fidelity.

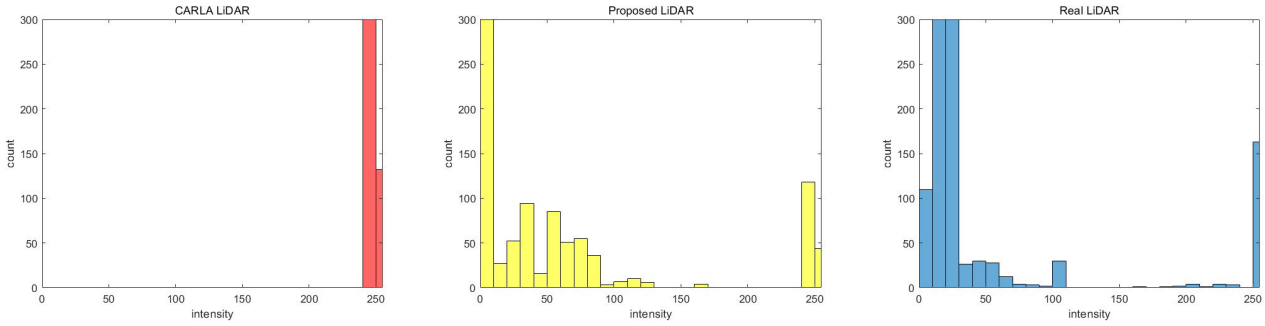

FIGURE 17. Intensity cumulative distribution by fidelity comparison experiment: (a) CARLA Lidar, (b) Proposed Lidar, (c) Real Lidar.

TABLE 4. Intensity difference by fidelity comparison experiment.

	CARLA Lidar	Proposed Lidar	Real Lidar
Number of Point	2761	2736	1537
Total intensity	674388	69477	71788
Average intensity	244.344	25.403	46.7370

In light of these observations, we sought to systematically evaluate the improvement in average intensity performance of the proposed lidar method relative to the conventional CARLA lidar. The absolute error from the real lidar measurements was calculated for each model, defined as the absolute difference between the model and real values. For the CARLA lidar, this computation involved taking the absolute difference between 244.344 and 46.737, which resulted in an absolute error of 197.607. Conversely, the proposed lidar yielded an absolute error of 21.334, derived from the absolute difference between 25.403 and 46.737.

Subsequently, we determined the percentage improvement in error of the proposed method relative to the CARLA lidar, as calculated using Equation (2).

$$I = \left(1 - \frac{Proposed\ error}{CARLA\ error}\right) \times 100 \tag{2}$$

Based on Equation (2), the improvement percentage is approximately 89.21%. This highlights that the proposed lidar method realizes an approximate 89.21% reduction in error in average intensity measurements when compared with the CARLA lidar.

V. CONCLUSION

In this paper, we have analyzed the lidar system focusing on the lidar sensor model to reduce the discrepancies between driving simulators and reality. Specifically, we investigated the impact of surface reflectance characteristics and surface color of the lidar measurement model, and proposed a virtual lidar system with a consideration of the effects of weather conditions. By comparing the proposed method to conventional lidar modeling techniques in a measurement experiment environment, we demonstrated that our approach could reduce the differences with real lidar measurements. Notably, in the ROI concerning average intensity, we observed an 89.21% improvement in performance compared to traditional modeling methods. The diffuse reflectance properties and brightness of surface colors were not used in the proposed method. Moreover, the weather parameters of the simulator are not quantitative, making it challenging to apply the method to other simulators. Despite these limitations, our approach utilizes object information within the simulator and the high real time performance of the ray-casting technique, enabling more realistic lidar outputs with lower computing power. By incorporating the effects of reflection angles on object surfaces, it is expected that the implementation fidelity of the proposed virtual lidar system can be further improved.

REFERENCES

[1] W. Zong, C. Zhang, Z. Wang, J. Zhu, and Q. Chen, "Architecture design and implementation of an autonomous vehicle," *IEEE Access*, vol. 6, pp. 21956–21970, 2018, doi: 10.1109/ACCESS.2018.2828260.
[2] T. D. Son, A. Bhave, and H. Van der Auweraer, "Simulation-based testing framework for autonomous driving development," in *Proc. IEEE Int. Conf. Mechatronics (ICM)*, Ilmenau, Germany, Mar. 2019, pp. 576–583, doi: 10.1109/ICMECH.2019.8722847.
[3] G. Bhatti, H. Mohan, and R. Raja Singh, "Towards the future of smart electric vehicles: Digital twin technology," *Renew. Sustain. Energy Rev.*, vol. 141, May 2021, Art. no. 110801, doi: 10.1016/j.rser.2021.110801.
[4] J. P. Allamaa, P. Patrinos, H. Van der Auweraer, and T. D. Son, "Sim2real for autonomous vehicle control using executable digital twin," *IFAC-PapersOnLine*, vol. 55, no. 24, pp. 385–391, 2022, doi: 10.1016/j.ifacol.2022.10.314.
[5] A. El Sallab, I. Sobh, M. Zahran, and N. Essam, "LiDAR sensor modeling and data augmentation with GANs for autonomous driving," May 2019, *arXiv:1905.07290*, doi: 10.48550/arXiv.1905.07290.
[6] A. Haider, M. Pigniczki, M. H. Köhler, M. Fink, M. Schardt, Y. Cichy, T. Zeh, L. Haas, T. Poguntke, M. Jakobi, and A. W. Koch, "Development of high-fidelity automotive LiDAR sensor model with standardized interfaces," *Sensors*, vol. 22, no. 19, p. 7556, Oct. 2022, doi: 10.3390/s22197556.

[7] R. Roriz, J. Cabral, and T. Gomes, "Automotive LiDAR technology: A survey," *IEEE Trans. Intell. Transp. Syst.*, vol. 23, no. 7, pp. 6282–6297, Jul. 2022, doi: 10.1109/TITS.2021.3086804.
[8] P. Rosenberger, M. Holder, M. Zirulnik, and H. Winner, "Analysis of real world sensor behavior for rising fidelity of physically based LiDAR sensor models," in *Proc. IEEE Intell. Vehicles Symp. (IV)*, Changshu, China, Jun. 2018, pp. 611–616, doi: 10.1109/IVS.2018.8500511.
[9] A. Schaermann, A. Rauch, N. Hirsenkorn, T. Hanke, R. Rasshofer, and E. Biebl, "Validation of vehicle environment sensor models," in *Proc. IEEE Intell. Vehicles Symp. (IV)*, Los Angeles, CA, USA, Jun. 2017, pp. 405–411, doi: 10.1109/IVS.2017.7995752.
[10] P. Rosenberger, M. Holder, S. Huch, H. Winner, T. Fleck, M. R. Zofka, J. M. Zollner, T. D'hondt, and B. Wassermann, "Benchmarking and functional decomposition of automotive LiDAR sensor models," in *Proc. IEEE Intell. Vehicles Symp. (IV)*, Paris, France, Jun. 2019, pp. 632–639, doi: 10.1109/IVS.2019.8814081.
[11] C. Linnhoff, P. Rosenberger, and H. Winner, "Refining object-based LiDAR sensor modeling—Challenging ray tracing as the magic bullet," *IEEE Sensors J.*, vol. 21, no. 21, pp. 24238–24245, Nov. 2021, doi: 10.1109/JSEN.2021.3115589.
[12] A. Hata and D. Wolf, "Road marking detection using LiDAR reflective intensity data and its application to vehicle localization," in *Proc. 17th Int. IEEE Conf. Intell. Transp. Syst. (ITSC)*, Qingdao, China, Oct. 2014, pp. 584–589, doi: 10.1109/ITSC.2014.6957753.
[13] Z. Wang, X. Wang, B. Fang, K. Yu, and J. Ma, "Vehicle detection based on point cloud intensity and distance clustering," *J. Phys., Conf. Ser.*, vol. 1748, no. 4, 2021, Art. no. 042053, doi: 10.1088/1742-6596/1748/4/042053.
[14] CARLA. *CARLA Components, Development and Installation Document*. Accessed: Aug. 20, 2023. [Online]. Available: https://carla.readthedocs.io/en/latest/
[15] Ibeo. *LUX 2010 User Manual*. Accessed: Mar. 2, 2023. [Online]. Available: https://github.com/AaronLK/libibeo
[16] Velodyne. *VLP-16 User Manual*. Accessed: Mar. 2, 2023. [Online]. Available: https://velodynelidar.com/wp-content/uploads/2019/12/63-9243-Rev-E-VLP-16-User-Manual.pdf
[17] J. R. Vargas Rivero, T. Gerbich, V. Teiluf, B. Buschardt, and J. Chen, "Weather classification using an automotive LiDAR sensor based on detections on asphalt and atmosphere," *Sensors*, vol. 20, no. 15, p. 4306, Aug. 2020, doi: 10.3390/s20154306.
[18] A. Filgueira, H. González-Jorge, S. Lagüela, L. Díaz-Vilariño, and P. Arias, "Quantifying the influence of rain in LiDAR performance," *Measurement*, vol. 95, pp. 143–148, Jan. 2017, doi: 10.1016/j.measurement.2016.10.009.
[19] M. Kutila, P. Pyykonen, H. Holzhuter, M. Colomb, and P. Duthon, "Automotive LiDAR performance verification in fog and rain," in *Proc. 21st Int. Conf. Intell. Transp. Syst. (ITSC)*, Maui, HI, USA, Nov. 2018, pp. 1695–1701, doi: 10.1109/ITSC.2018.8569624.
[20] *Matlab User Manual, LiDAR Motion Compensation*. Accessed: Mar. 2, 2023. [Online]. Available: https://kr.mathworks.com/help/lidar/ug/motion-compensation-in-lidar-point-cloud.html#MotionCompensationIn3DLidarPointCloudsUsingSensorFusionExample.
[21] D.-J. Lee, J. Im, and J.-H. Won, "A study on virtual LiDAR sensor simulation method for autonomous driving simulator," in *Proc. Korea Intell. Transp. Syst. Conf.*, Jeju, South Korea, Jun. 2022, pp. 1131–1134.

DONG-JU LEE received the B.S. degree from Kyungil University, in 2021. He is currently pursuing the M.S. degree with the Autonomous Navigation Laboratory, Inha University, South Korea. His research interests include self-driving cars and driving simulator.

JIUNG IM (Graduate Student Member, IEEE) received the B.S. and M.S. degrees from Inha University, South Korea, in 2018 and 2020, respectively, where he is currently pursuing the Ph.D. degree with the Autonomous Navigation Laboratory. His research interests include self-driving cars and driving simulator.

JONG-HOON WON (Member, IEEE) received the Ph.D. degree from the Department of Control Engineering, Ajou University, South Korea, in 2005. He was with the Institute of Space Application, University Federal Armed Forces (UFAF), Munich, Germany. He was nominated as the Head of the GNSS Laboratory, Institute of Space Application, in 2011, and has been involved in lectures on advanced receiver technology with the Technical University of Munich (TUM), since 2009. He is currently an Associate Professor with the Department of Electrical Engineering, Inha University. His research interests include GNSS signal design, receiver, navigation, target tracking systems, and self-driving cars.